Theoretical and in-situ FTIR study of the atmospheric sink for the reaction of methyl dichloroacetate (MDCA) with ·OH and Cl· radicals: kinetics, product distribution and mechanism.

Abstract:

The atmospheric degradation of methyl dichloroacetate initiated by ·OH and Cl· radicals can occur via H-atom abstraction from the alkyl groups, (Cl_2HC– or $–CH_3$). The product yields for the gas phase reaction with ·OH were determined experimentally in a 480 L Pyrex glass atmospheric-simulation reactor coupled to an *in-situ* Fourier transform infrared (FTIR) spectrometer. In addition to those results, we present in this paper a complete degradation mechanism, based on thermodynamic data obtained by identifying all critical points on the potential-energy surface for said reactions, employing density functional calculations with the M06-2X and MN15 hybrid exchange-correlation functionals and the aug-cc-pVTZ basis sets. A conformational search for reactants and transition states was performed. The energies of these conformers were later corrected at the CCSD(T,Full)-F12/CBS level using the SVECV-f12 composite method. The corrected energies were then used to obtain the theoretical rate coefficients in a multi-conformer approach. The products and their yields for the reaction with ·OH were $Cl_2CHCOOH$ (44±3%), $COCl_2$ (43±3%), and CO (41±6%). The analysis of the mechanism suggests that formation of P1 (Cl_2CO, phosgene) occurs mainly by abstraction from the Cl_2HC– group, since the formation of P4 ($Cl_2CHC(O)OH$, dichloroacetic acid) and P5 (CO, carbon monoxide) are more favorable in the path for abstraction from the $–OCH_3$ group. The multi-conformer calculated rate constants values were compared with the values obtained employing only the low-lying TS's and with our own previous experimental studies. Branching ratios for the reaction with ·Cl were compared with the experimental yields of products.

Keywords: Methyl dichloroacetate, Fourier transform infrared, Potential-Energy Surface, Volatile Organic Compounds, Atmospheric oxidants**.**

1. Introduction

Environmental concerns about the fate of Volatile Organic Compounds (VOCs) released into the atmosphere by anthropogenic sources –mainly due to population growth and industrialization– have increased greatly in recent decades. Once emitted, VOCs are subject to various forms of physical or chemical elimination in the troposphere. This may occur because of wet or dry deposition, for instance, or because of chemical transformations as the photooxidation initiated by •OH radicals, •Cl atoms, NO_3 and O_3 molecules, which essential mechanisms are hydrogen atom abstraction or addition to double bonds.(Finlayson-Pitts and Pitts Jr, 1999)

As a result of these chemical transformations, several compounds can be produced that have the same or larger atmospheric impact than the primary species. This is the case, for example, for methyl dichloroacetate ($CHCl_2$–$CC(O)OCH_3$, MDCA), which could be generated by the atmospheric oxidation of some ethers or released from the earth's surface.(Terao, 1992) MDCA is widely used as chemical component in disinfection products, protective coatings, and varnishes, and as starting reagent for obtaining pharmaceutical and agrochemical products.(McClay et al., 2007)

Exploring the mechanism, determining products, and getting kinetic data for those chemical transformations is essential for a better understanding of their environmental impact. For this purpose, the computational tools of theoretical chemical modeling are extremely useful. If experimental information on a chemical reaction is available, then the theoretical kinetic study could be used to verify the reliability of the proposed mechanism and the accuracy of the results obtained. On the other hand, if no experimental data is available, computational calculations can be used to select more confidently the appropriate conditions to conduct the experimental investigation.

In the case of MDCA, Straccia et al. 2023(Straccia C et al., 2023) have obtained experimental kinetic and product-distribution data for the degradation reaction with •Cl atoms under quasi-real atmospheric conditions. However, there were no experimental data reported for the reaction initiated by •OH radicals.

We report in this work the experimental product distribution of MDCA for the reaction with OH under atmospheric conditions using *in-situ* FTIR spectroscopy. In addition, electronic structure calculations were used to develop a detailed mechanism for the oxidation of MDCA both by •OH and Cl• radicals, using DFT methods to study the structure of reactants, intermediates, transition states and products. Moreover, more accurate energy evaluations were also conducted using the recent SVECV-f12 composite method, as explained later, and those energies were used to calculate theoretical rate coefficients that were then compared to the experimental ones.

To the best of our knowledge, this work presents the first experimental product distribution and product yields of MDCA in the reaction with •OH, as well as the first theoretical study of the atmospheric oxidation of MDCA by •Cl atoms. This data can be used to estimate the possible environmental implication of the emission and subsequent atmospheric oxidation of MDCA.

2. Materials and methods

2.1. Experimental determination of the products

All the experiments were performed at 1000 mbar of synthetic air and (298 ± 2) K in a Pyrex simulation chamber of 480 L surrounded by 32 fluorescence lamps. These emit at a maximum of 360 nm to produce the corresponding radicals. The chamber is coupled to a FTIR spectrometer used for the analysis. A system of "White" type mirrors accounts for multiple internal reflections, thus increasing the optical path and allowing the use of low concentrations of the reactants, similarly to the conditions in which they are found

in the atmosphere. A full description of the reactor can be found in the literature.(Barnes et al., 1994) •OH radicals were produced by photolysis of CH_3ONO (see the Supporting Information, SI).

The product studies were performed on MDCA/OH/synthetic air mixtures that were irradiated using fluorescent lamps. Product identification and quantification were developed by comparison to calibrated reference spectra database belonging to the laboratory.

2.2. Materials

The initial concentration of MDCA used in the experiments was around 10 ppm (1 ppm=2.46×10^{13} molecule/cm^3 at 298 K and 760 Torr of total pressure). Chemicals were used as supplied by the manufacturer (purity is given in parenthesis): synthetic air (Air Liquid, 99.999%), nitrogen (Air Liquid 99.999%), methyl dichloroacetate (Sigma-Aldrich, 99%), and nitric oxide (Messer Griesheim, 99%).

2.3. Electronic structure calculations

Optimized geometries for MDCA and other structures on the potential energy surface (PES) were obtained at the Kohn-Shan density functional theory (KS-DFT) level employing the M06-2X and MN15 hybrid exchange-correlation functionals, which show a reasonable accuracy/cost benefit relationship for barrier heights.(Goerigk et al., 2017; Kohn and Sham, 1965; Yu et al., 2016; Zhao and Truhlar, 2008) Dunning´s cc-pVTZ and aug-cc-pVTZ basis sets, and the empirical Grimme dispersion (D3, for M06-2X) were employed for the calculations.(Grimme et al., 2010; Woon and Dunning, 1995, 1993) Rigid-Rotor Harmonic Oscillator (RRHO) vibrational analyses was carried out at the optimized geometries to obtain thermodynamic properties for all species and verify the absence of imaginary frequencies for local minima or the presence of a single imaginary frequency for transitions states (TS). Intrinsic reaction coordinate (IRC) scans were conducted to confirm the connectivity for transition states and local minima. The

coordinates, vibrational frequencies, and moments of inertia of the optimized structures are provided in the SI. DFT calculations were performed using the Gaussian 16 software package.(Frisch et al., 2016)

2.4. Rate constant calculations

The height of the barriers is a crucial property of reaction paths on the PES. Due to its presence in the exponential function, a very accurate calculation of the barriers, beyond what DFT can afford, is necessary. To reach this accuracy, we employed the recently developed SVECV-f12 composite method which was shown to give excellent results in different situations.(Kieninger and Ventura, 2022; Ventura et al., 2021) This protocol uses the M06-2X-D3 method for geometry optimization and frequencies evaluation, while the final accurate energy is computed at the optimum geometries by the explicitly correlated CCSD(T)-F12 method(Adler et al., 2007; Knizia et al., 2009) extrapolated to the complete basis set (CBS) limit using the cc-pVDZ-F12 and cc-pVTZ-F12 basis sets.(Peterson et al., 2008) Finally, the core valence correlation energy is also included by employing the MP2 method with the cc-pVCTZ basis set.(Woon and Dunning, 1995) The SVECV-f12 composite method has been tested specifically for the prediction of barriers of reaction for several archetypical systems(Kieninger and Ventura, 2022; Ventura et al., 2021) and found to produce results with an accuracy of 0.5 kcal/mol or better, in comparison with experiment and/or more sophisticated and expensive methods of calculation. The CCSD(T)-F12 calculations necessary for this method were performed using the Molpro 2020.1 computer program.(Werner et al., 2020) Canonical transition state theory (TST) was employed to determine calculated rate constants, To enhance the accuracy of results and provide a more comprehensive description of the chemical reaction space, the CREST program(Grimme, 2019; Pracht et al., 2020) was employed to identify the low-lying transition state (TS) conformations. Additionally for comparison purposes, Anharmonic frequency analysis at the optimized geometries of reactants and transitions states was performed. Eckart(Eckart,

110 1930) tunnelling correction factor was calculated using the KiSThelP software package.(Canneaux et al.,
111 2014)

112 3. Results and discussion

113 3.1. Products

114 The atmospheric degradation of MDCA by •OH radicals occur via H-atom abstraction from the alkyl
115 groups, (Cl_2HC or CH_3). After the abstraction, O_2 addition produce peroxy radicals (ROO•) that would
116 react with •NO or other peroxy radicals to form alkoxy radicals (RO•). These RO• can react along several
117 paths: 1) with O_2 to form a polyfunctional compound, 2) decompose through C-C or C-O bond cleavage,
118 or 3) undergo an α-ester rearrangement with further decomposition to form a carboxylic acid and other
119 smaller radical. **Figure 1 1** shows the IR spectra acquired before (spectrum i) and after (spectrum ii) UV
120 irradiation of the MDCA/CH_3ONO/air/NO mixture. Spectra iii) and iv) are the reference IR of
121 dichloroacetic acid ($Cl_2CHCOOH$) and phosgene ($COCl_2$), respectively. v) is the residual spectrum
122 obtained after subtraction of the IR spectra mentioned before and those of NO_2, NO, CO_2, CO, CH_3ONO,
123 and HCHO.

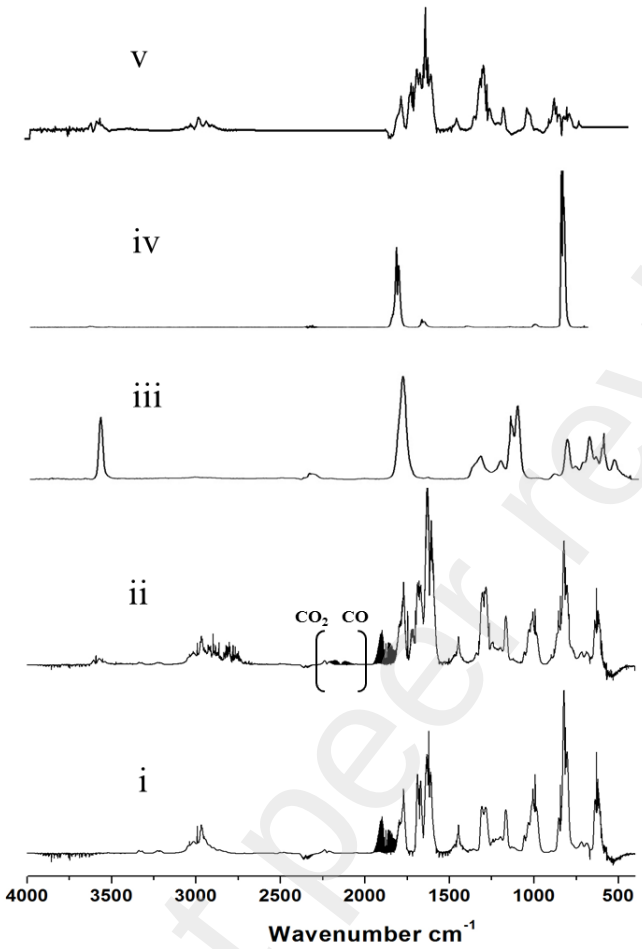

Figure 1 IR spectra (i) before and (ii) after 25 minutes of irradiation of a mixture MDCA/CH_3ONO/air. Traces (iii) and (iv) show reference spectra of dichloroacetic acid ($Cl_2CHCOOH$) and phosgene ($COCl_2$), respectively. Trace (v) shows the residual spectrum obtained after subtraction of features belonging to NO_2, NO, CO_2, CO, CH_3ONO, and HCHO, (iii) and (iv) from the spectrum in trace (ii)

Figure 2a shows the concentration-time profiles for the reaction of MDCA with •OH radicals and the products formed. **Figure 2b** shows plots of products formation *versus* loss of methyl dichloroacetate. These plots are linear with near zero intercepts and least squares analyses of the slopes show yields of (*44* ± *3*)%, (*43* ± *3*)%, and (*41* ± *6*)% for $Cl_2CHCOOH$, CCl_2O, and CO respectively (see the SI). The errors shown are a combination of the 2σ statistical error from the regression analysis.

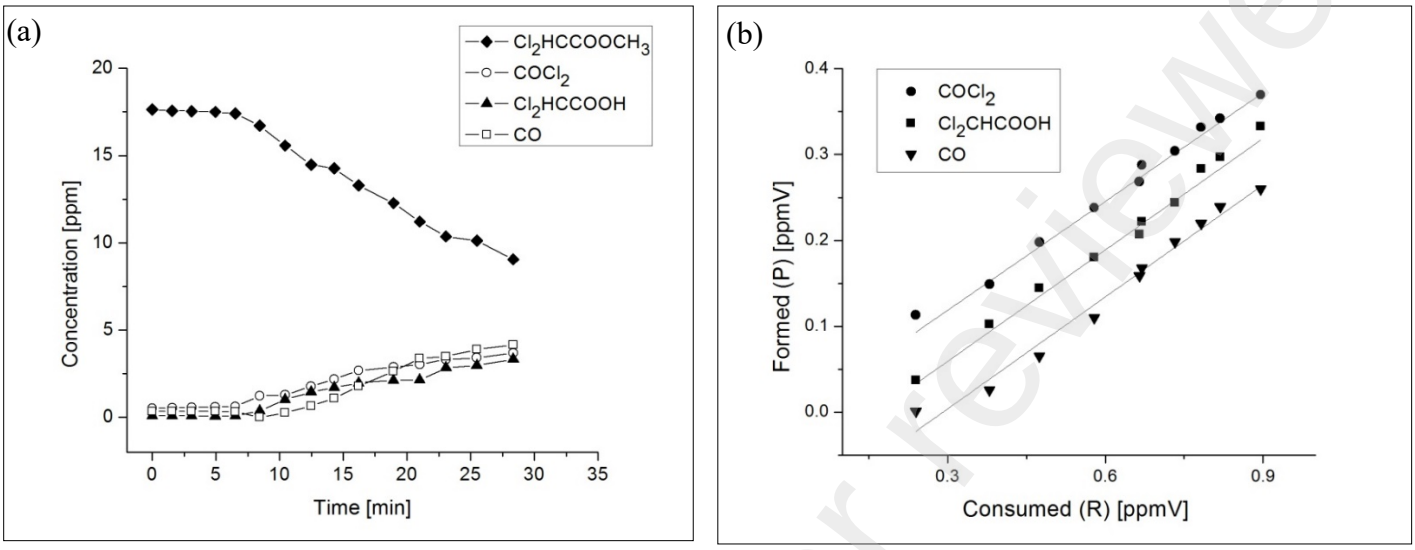

Figure 2 Plots of experimental data from the gas phase reaction of MDCA with ˙OH radicals at atmospheric pressure of synthetic air and 298 K. (a) Concentration-time profiles (b) products formation versus loss of MDCA

3.2. MDCA optimized geometry.

Geometry optimization provides information about the bond lengths, bond- and dihedral angles in the molecule. It helps to understand the spatial arrangement of atoms, the presence of any steric interactions, and the overall molecular shape, which can have implications for reactivity and chemical properties. In the case of MDCA, there are three single bonds ($CHCl_2$–C, CH_3O–C and CH_3–O) around which the groups can rotate overcoming small conformational barriers. The geometry optimization afforded four conformers that are shown in **Figure 3** (XYZ coordinates of all species are given in the SI).

The MDCA molecule has four minimum energy conformation due to the internal rotation on the **H-C1**(Cl_2)-**C2**(OCH_3)-**O** (φ_1) and **O-C2**($CHCl_2$)-**O**-**C**H_3 (φ_2) dihedral angles, with the φ_1=*0°*, φ_2=*0°* conformation (**MDCA_1**) as the global minimum. The energies in the following will be expressed in ZPE energies relative to the **MDCA_1** conformer at the M06-2X/D3/aug-cc-pVTZ (M06) and MN15/aug-cc-

pVTZ (MN15, inside Brackets) levels of theory, other thermodynamic quantities are included in the SI. The conformations φ_1=*151.1°*, φ_2=*2.6°* (**MDCA_2**), φ_1=*0°*, φ_2=*173.8°* (**MDCA_3**) and φ_1=*-144.2°*, φ_2=*174.9°* (**MDCA_4**) are *0.55[49]*, *7.75[7.11]* and *8.74[8.12]* kcal/mol over the **MDCA_1** conformation, respectively, in agreement with the minimal conformations described in previous calculations.(Gnanaprakasam et al., 2018; Litvinov et al., 1993) Based on the energy differences between conformers and the calculated the Boltzmann thermal distribution of conformers (see the SI) the **MDCA_1** and **MDCA_2** conformations contribute around 98.8% to the equilibrium population at working temperature (298 K), only these conformers will be considered in the subsequent sections.

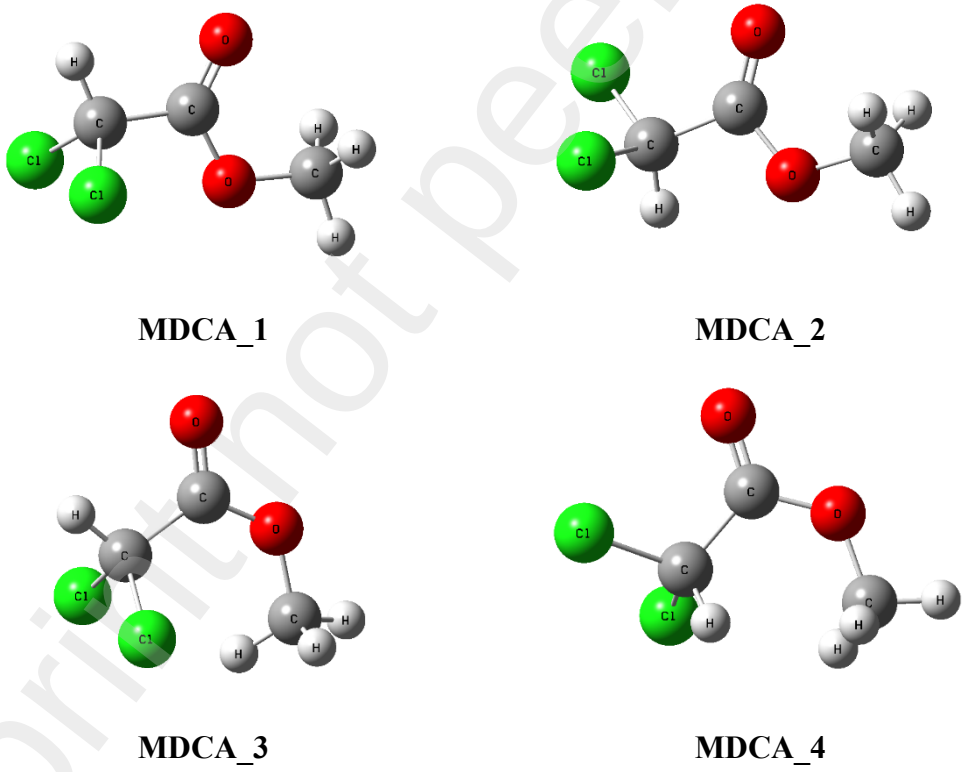

Figure 3 Optimized geometries of the MDCA conformers at the M06-2X/D3/aug-cc-pVTZ level of theory.

3.3. MDCA Gas-phase Oxidation Mechanism

Based on our results, the rate determining step in the gas phase oxidation of MDCA is the H-abstraction by atmospheric radicals. The MDCA molecule has two positions for H-abstraction, the Cl_2HC– and –OCH_3 groups (with X=$^{\bullet}$OH, $^{\bullet}$Cl):

$$Cl_2HCC(O)OCH_3 + X^{\bullet} \rightarrow {}^{\bullet}CCl_2C(O)OCH_3 \text{ (IM1)} + HX \quad (1)$$

$$Cl_2HCC(O)OCH_3 + X^{\bullet} \rightarrow Cl_2HCC(O)OCH_2{}^{\bullet} \text{ (IM2)} + HX \quad (2)$$

Under atmospheric conditions, once H-abstraction has occurred, the radical intermediates **IM1** and **IM2** will react further with O_2 to produce $RO_2^{\bullet}$ radicals that eventually evolve toward $RO^{\bullet}$ radicals by recombination with other species ($RO_2^{\bullet}$, $^{\bullet}$NOx, or $^{\bullet}$OH).(Atkinson, 2007; Bossolasco et al., 2014; Faragó et al., 2015; Fittschen et al., 2014) The decomposition of $RO^{\bullet}$ intermediates into simpler products will be described in section 3.

3.3.1. MDCA + $^{\bullet}$OH

The first step in the H-abstraction mechanism from Cl_2HC– group is the formation of a pre-reactive complex (**PRC1OH**, *-4.7[-4.81]* kcal/mol, in which the $^{\bullet}$OH radical is located on the same plane of the H-C-C=O atoms on MDCA stabilized by hydrogen bonding with distances between OH···O=C and HO···HC of *1.93* and *2.44* Å, respectively (**Figure 4**). In the transition state (**TS1OH**, *-0.47[-1.38]* kcal/mol), the HO···HC distance along the reaction path is reduced to *1.33* Å and the C–H bond in MDCA increases from *1.08* to *1.19* Å forming a six-membered transition state for H-abstraction. Notice that, albeit by a small energy, the TS is submerged with respect to the reactants, but still about *4* kcal/mol over the pre-reactive complex. This barrier, which once surmounted leads to the intermediates **IM1**+H_2O (*-35.2[-37.4]* kcal/mol), is slightly lower that the energy necessary to return to reactants. The height of the barrier and the exothermicity of the intermediate imply that the reaction will occur in this direction, both from the kinetic and thermodynamical points of view.

As in the H-abstraction mechanism from Cl_2HC–, in the –OCH_3 group a hydrogen bonded pre-reactive complex (**PRC2OH**, *-5.1[-4.8]* kcal/mol) is also formed. The reaction then proceeds along the path for H-abstraction via a seven-membered TS (**TS2OH**, *0.6[0.16]* kcal/mol) in which the OH···O=C and HO···HC bond distances are modified from *1.95* to *2.26* Å, and *2.56* to *1.33* Å, as the reaction proceed. The **TS2OH** barrier from **PRC2OH** (*5.7[4.9]* kcal/mol), is about 1.7 kcal/mol larger than that of **TS1OH** on the other abstraction path. The larger barrier and the not so deep well for the intermediate **IM2** + H_2O *(-23.8[-24.9]* kcal/mol), as shown in **Figure 4**, implies that the H-abstraction from Cl_2HC–is both thermodynamically and kinetically more probable than the same from –OCH_3 group. Both geometries and energies calculated in this work show good agreement with the corresponding theoretical values reported previously at the M06-2X/6-311++G(2df,2p) level of theory.(Gnanaprakasam et al., 2018)

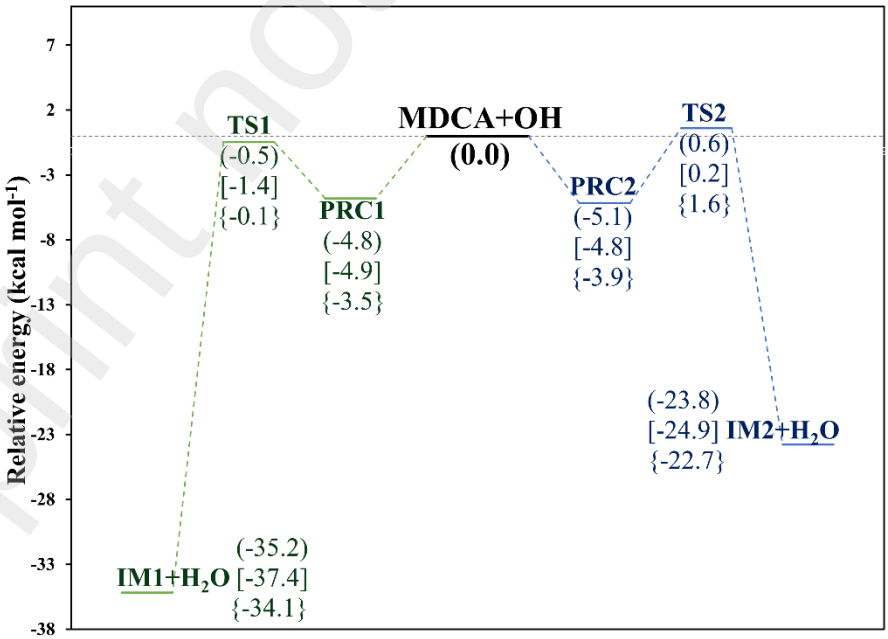

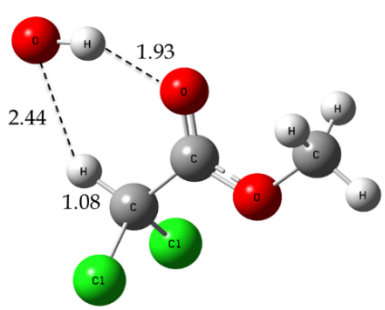

PRC1OH

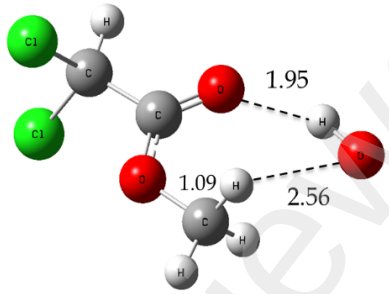

PRC2OH

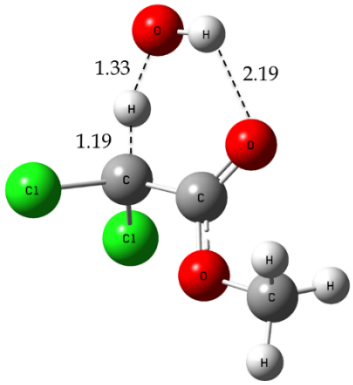

TS1OH

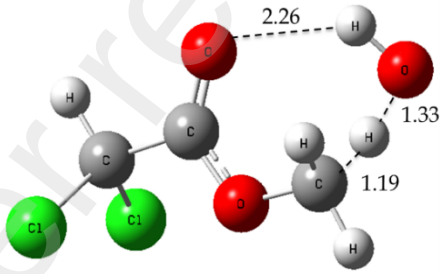

TS2OH

Figure 4 H-abstraction on the MDCA gas phase oxidation initiated by OH radicals. (***up***) Partial relative energy diagram (ZPE corrected) at the (M06), [MN15] and {SVECV-f12} levels of theory (kcal/mol). (***middle and down***) Optimized geometries for prereactive complex and transition states at the M06-2X-D3/aug-cc-pVTZ level of theory.

187

One of the important things in considering theoretical calculations is their precision. That means that, if sufficiently accurate methods are used, the results should not show large difference (i.e., precision of the predictions). In this work we used MN15 and SVECV-f12 in addition to M06-2X-D3, and we can compare the energies obtained with those methods. For instance, **PC1OH**, which lies at *-4.7* kcal/mol at the M06-2X-D3 level, appears at *-4.8* and *-3.4* kcal/mol at the other two levels of theory, while the transition state **TS1OH** appears at *-0.5*, *-1.4* and *-0.1* kcal/mol, respectively. The barriers then are *4.3*, *3.5* and *3.4* kcal/mol supporting not only the fact that the methodology is precise, but also that the numbers converge when the sophistication level of the theory is increased. A similar situation occurs for all the other minima and transition states calculated in this paper.

3.3.2. MDCA +• Cl

Figure 5 shows the energetics for the reaction of MDCA with •Cl atoms. In this case, the H-abstraction from the Cl_2HC– group occurs directly from the reactants without formation of any pre-reactive complex. There is a non-submerged transition state **TS1Cl** with a very small barrier of *0.18[-2.6]* kcal/mol (*1.24* kcal/mol at the SVECV-f12 level) and the relative energy of the intermediates (**IM1**+ HCl in this case) is *-18.5[-22.9]* kcal/mol. On the other side, the abstraction from the $–OCH_3$ group lead first to the formation of a pre-reactive complex **PRC-Cl** (*-3.9[-4.0]* kcal/mol and *-2.6* kcal/mol at the SVECV-f12 level) as can be seen in **Figure 5.**

In **PRC-Cl**, the incoming chlorine atom is on top of the MDCA molecule, interacting both with the C=O and C-H bonds and almost perpendicular to the C1–C2–O–C3 plane. The angle to the carbonyl group (C=O···Cl) is *103.8* degrees, and the distances Cl···O and Cl···HC are *2.73* and *2.85* Å, respectively. From this pre-reactive complex, the reaction path continues by a movement of the Cl atom toward the $–OCH_3$ group, decreasing the Cl···HC distance to *1.49* Å in the transition state **TS2Cl**. This TS is submerged by

1.1[1.3] kcal/mol and the barrier height for this path is *2.8[2.7]* kcal/mol with the intermediates **IM2**+HCl exergonic by *7.46[-10.9]* kcal/mol (see **Figure 5**). The experimentally observed product $Cl_3C(O)OCH_3$ clearly comes from the reaction of the intermediate **IM1** with Cl which is readily explainable both by the almost non-existent barrier and the much less stable **IM2** species. Although the abstraction from the $-OCH_3$ group seems to be kinetically more favorable (**TS2Cl** at *-1.2* kcal/mol *vs.* **TS1Cl** at *+0.1* kcal/mol) the large production of $Cl_3C(O)OCH_3$ determined experimentally(Straccia C et al., 2023) can be easily explained thermodynamically by the very large differences in stability between **IM1** and **IM2**. Nonetheless, secondary products coming from path 2 should not be totally negligeable.

Notice that once the very stable **IM1** intermediate is formed, it can react with Cl, as described in the previous paragraph, in case there is a high concentration of chlorine atoms, but it can also react further with an oxygen molecule to form the $RO_2^{\bullet}$ peroxy radical. This route will be described later, in section 3. Let us just advance here that the barrier for Cl addition is about *2* kcal/mol lower than that for the addition of the oxygen molecule, thus explaining the observed experimental result.(Straccia C et al., 2023)

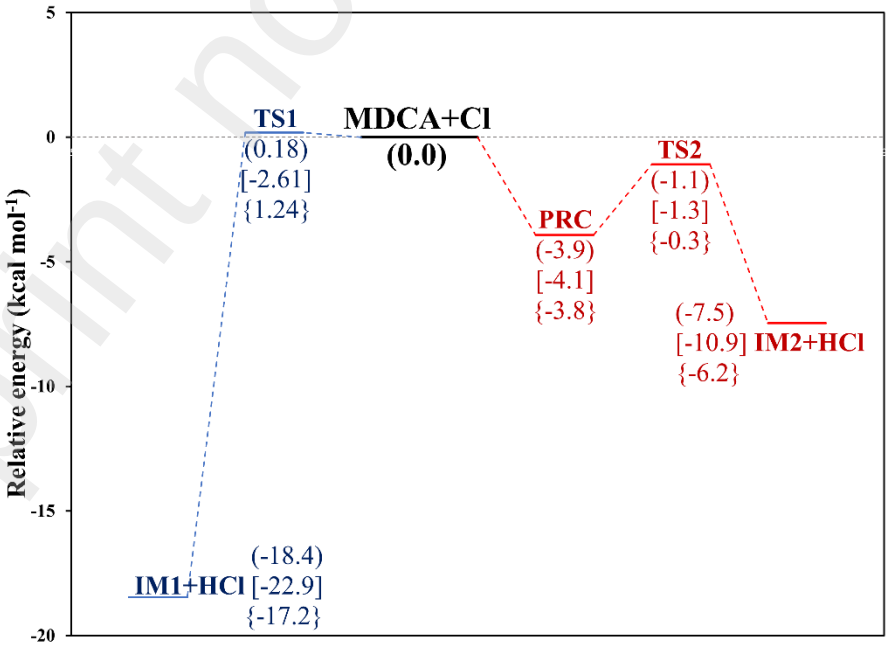

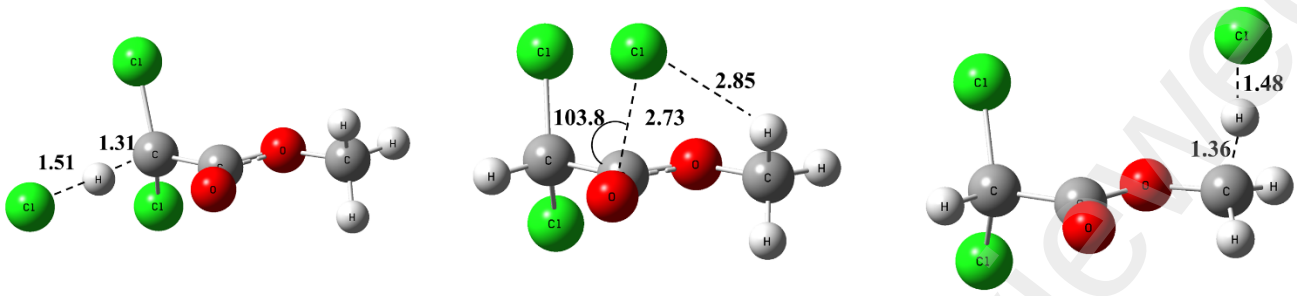

TS1Cl **PRC** **TS2Cl**

Figure 5 H-abstraction on the MDCA gas phase oxidation initiated by Cl atoms. (***up***) Partial relative energy diagram (ZPE corrected) at the (M06), [MN15] and {SVECV-f12} levels of theory (kcal/mol). (***down***) Optimized geometries for prereactive complex and transition states at the M06-2X-D3/aug-cc-pVTZ level of theory.

As mentioned before, to calculate theoretical rate coefficients for the initial H-abstraction on MDCA at standard room temperature (298 K), the energy of the critical points on the PES optimized at the M06 and MN15 levels of theory was corrected by using the SVECV-f12 composite method. As a pre-reactive complex is formed before the H-abstraction reaction in three of the four paths, the relative scheme can be written as follows:

$$\text{MDCA} + \text{X} \rightarrow \text{PRC} \qquad k_{PRC}$$

$$\text{PRC} \rightarrow \text{MDCA} + \text{X} \qquad k_{-PRC}$$

$$\text{PRC} \rightarrow \text{Products} \qquad k_{TS}$$

For both OH and Cl H-abstractions, the barrier from PRC to products and PRC back to reactants is roughly the same (**Figure 4** and **Figure 5**), however, it is expected that the k_{-PRC} be higher than k_{TS} due the entropy for the reverse PRC→ R process, and the simplified approximation that the pre-reactive complex is at thermal equilibrium can be adopted (see **Table S1**). Then, the overall rate can be expressed as:

$$k = K_{PRC} \times k_{TS}$$

with K_{PRC} being the thermal equilibrium constant between reactants and PRC and k_{TS} is the rate constant for H-abstraction of each position (Cl_2HC– or –OCH_3) The expression for the rate constant contains values that correspond to the PRC in both K_{PRC} and k_{TS}. These values cancel each other out, which prevents us from calculating them and further simplifies the calculation of the rate constant.

The rate constants were computed for the most stable conformers of MDCA_1 and MDCA_2, as well as for the conformers of the low-lying transition states for each reaction, assuming thermal equilibrium at room temperature and that any of the TS could be accessible from either of the two MDCA conformers. The rate constant value of each MDCA and TS conformer was then weighted by its Boltzmann population (ρ) at 298K, according to the following expression:

$$k = \rho_{MDCA\_1} \sum_i \rho_i k_i + \rho_{MDCA\_2} \sum_i \rho_i k_i$$

In the reaction with Cl atoms, three conformers of TS were considered for Cl_2HC– and five for –OCH_3 groups. In contrast, the reaction with OH radicals considered four and six conformers for Cl_2HC– and –OCH_3 groups, respectively. The theoretical values of the rate coefficients for H-abstraction by •OH and •Cl radicals at the SVECV-f12 level of theory are:

$k_{1(OH)} = 9.43 \times 10^{-13}$ cm3/molecule·s (from Cl_2HC–),

$k_{2(OH)} = 1.31 \times 10^{-13}$ cm^3/molecule·s (from –OCH_3),

$k_{1(Cl)} = 0.73 \times 10^{-12}$ cm^3/molecule·s (from Cl_2HC–),

$k_{2(Cl)} = 6.61 \times 10^{-12}$ cm^3/molecule·s (from –OCH_3).

Several comments must be done on these numbers. In the first place, the global rate coefficient calculated for the reaction with chlorine atoms (7.34×10^{-12} cm^3/molecule·s) overestimate about twenty times ($k_{(SVECV\text{-}f12)} = 22 \times k_{(Exp)}$) the experimental value (3.31×10^{-13} cm^3/molecule·s)(Straccia C et al., 2023) despite the energy corrections with the SVECV-f12 composite method on the M06 geometries reduce the rate constant value by about 25% (therefore overestimation), Furthermore, the values presented above have the correction for tunneling added, which in fact increases the value of the constant (without the correction the relationship is $k_{(SVECV\text{-}f12)} = 8 \times k_{(Exp)}$) and the relationship between the global values of rate constants is $k_{(Cl)} = 7 \times k_{(OH)}$ even though the barriers are quite similar, supporting that the calculated rate constants are very sensitive to the reaction barriers and tunneling correction.

Although the value calculated for the rate constant with Cl atoms overestimates the experimental value. The multi conformer approach considerably improved its value with respect to the value calculated using only the low-lying TS for each path (1.77×10^{-11} cm^3/molecule·s). For the reaction with OH radicals this does not seem to be the case since the calculated reaction rate becomes faster when using the multi-conformer approach compared with the values for the low-lying TS (10.7×10^{-13} and 6.31×10^{-13} cm^3/molecule·s, respectively). The latter is in better agreement with those calculated previously (*2.07* and 0.28×10^{-13} cm^3/molecule·s).(Gnanaprakasam et al., 2018) However, at the time of writing this work there is no information available about the experimental value of the reaction with OH radicals, so comparisons cannot be made. However, given the usual relationship between the constants $k_{(Cl)}/k_{(OH)}$ we can assume that the overestimation may also be present on calculated rate reaction with OH radicals.

We calculated anharmonic corrections to thermodynamic properties and included those values in the supplementary information. The main effect of these corrections is a change in the distribution between conformers of the transition state (TS), and an increase in the reaction rate for both Cl atoms and OH radicals. However, we found that including anharmonicity does not improve the value of the rate constant.

Moreover, it greatly increases the time required for the calculation, making it impractical to use for systems with a greater number of atoms.The calculated branching ratio for the reaction with OH radicals were *88*% and *12*% for Cl_2HC– and –OCH_3, respectively, while in the reaction with chlorine atoms, the branching ratio is *10*% and *90*% estimating that meanwhile in the reactions with OH radicals the reaction occurs mainly by the Cl_2HC– group, on the reaction with Cl atoms most of the reaction would go through the abstraction from the –OCH_3 group, in contrast to the high yields reported experimentally for $Cl_3C(O)OCH_3$, suggesting that this yield can be biased by the high concentrations of chlorine atoms used experimentally.

There may be an alternative explanation though. In the case of chlorine, we explained before why the observed products is justified on thermodynamic grounds, not kinetic. If this is the case, then the reaction leading to **IM1** proceeds very fast, regardless that the transition state leading to **IM2** is lower. Then, the rate of reaction will not be determined by the relation between the transition states **TS1Cl** and **TS2Cl**, but from the height of the transition state for the reaction between **IM1** and the additional $^{\bullet}$Cl atom. In other words, the **IM1**/**IM2** equilibrium would be stablished very fast in favor of the first, and the competition between the reactions of **IM1** with O_2 and $^{\bullet}$Cl will stablish the real kinetics of the reaction. Let us then examine this aspect of the problem.

Certainly, something is missing, we have noticed a significant difference between the chosen DFTs, especially in the branching ratios and, although both overestimate the value of the constant, they do so to a different extent. Obviously, the choice of the calculation method greatly affects the results, although the energy correction with SVECV-f12 improves the results but is still dependent on the geometry and thermochemistry calculated at the DFT level where perhaps the error cancellation reaches its limit. In this work we have calculated the kinetics with two approaches. Using only the minimum energy conformers

of the MDCA molecule and its transition states, and using the main MDCA and TS conformers in a multi-conformer TST(Viegas, 2021) treatment which allow us to have values closer to the experimental.

3.3.3. RO• intermediates decomposition

The reactions of **IM1** and **IM2** with O_2 and additional Cl atoms (for MDCA + Cl reaction) are shown in **Figure 6**. Although the reaction between triplet O_2 and methylic radicals is usually barrierless, in fact the reaction between **IM1** and O_2 has a barrier of *4.1[2.1]* kcal/mol and occurs through a well-defined transition state (**TS1-1**, relative to **IM1** therein), further reacting to produce the alkoxy radical **IM1O** (this reaction occurs by the presence of NOx or reaction with other radicals, but this study has been omitted in the present work). The **IM1O** intermediate decomposes through a low energy transition state **TS1-2** (*-18.3[-17.3]* kcal/mol) of C1–C2 bond cleavage and leads to phosgene (Cl_2CO, **P1**) whose experimental yield was *43*%, and the methyl formate radical intermediate ($^{\bullet}C(O)OCH_3$, **IM3**). The latter decomposes through an O–C bond cleavage **TS1-3** (*-9.6[-7.1]* kcal/mol), to carbon dioxide (CO_2, **P2**) and methyl radical intermediate (**IM4**), which eventually produces formaldehyde (H_2CO, **P3**) and hydroperoxyl radicals ($HO_2^{\bullet}$) via successive reaction with O_2 (**Figure 6**). It should be noted that **P1** can be formed by both the abstraction channel in Cl_2HC– and the abstraction channel in $–OCH_3$ (see below). The determined value for **P1** yield drops from *43* to *19*% in the reaction of DMCA with chlorine atoms, this occurs together with the appearance of methyl trichloro acetate (**P7**, $Cl_3C(O)OCH_3$), formed by the addition of Cl atoms to **IM1** through a low barrier TS (*2.1[-1.7]* kcal/mol) for which an experimental yield of *44*% was reported. (Straccia C et al., 2023)

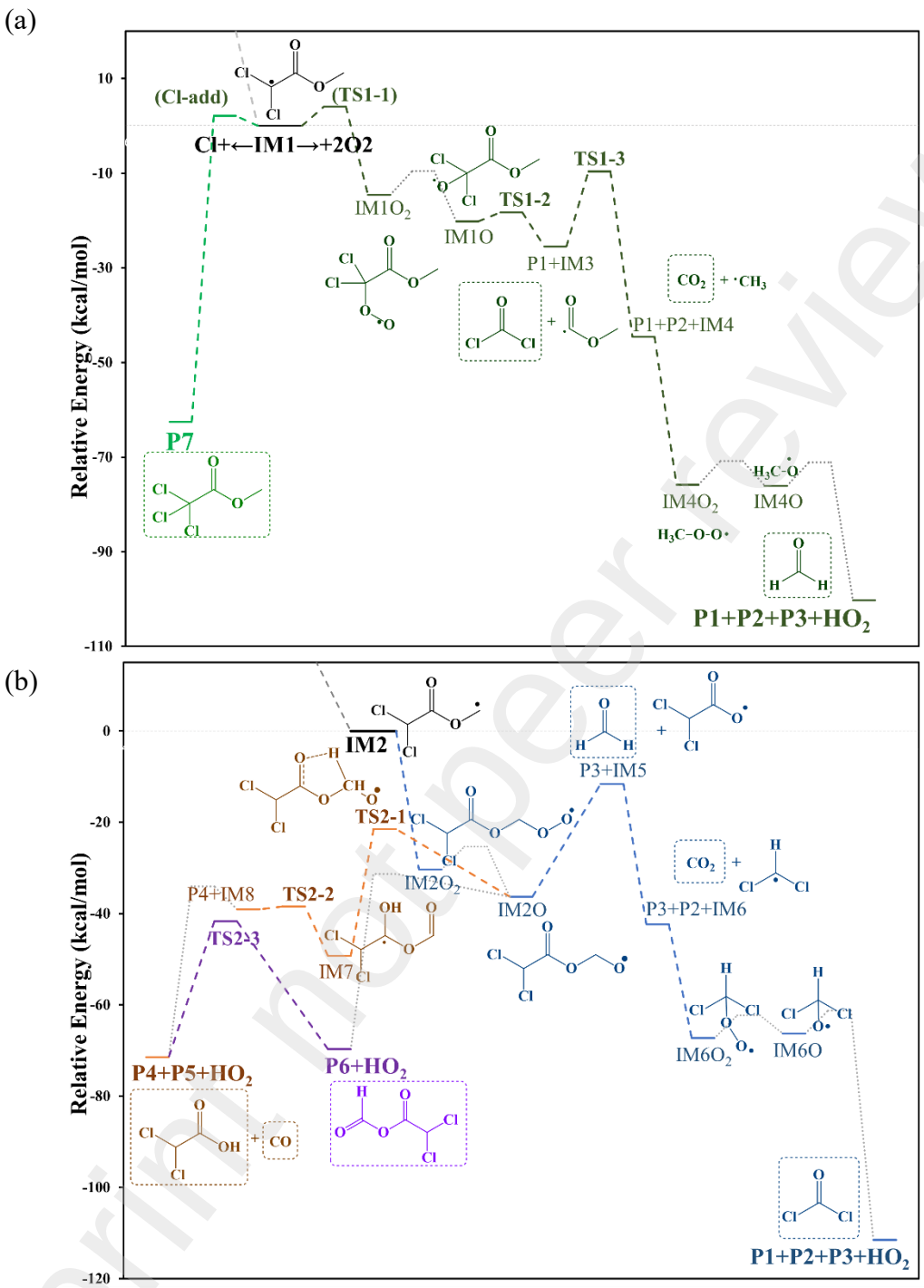

Figure 6 Relative energy diagram (ZPE corrected) for the RO• intermediates from MDCA oxidation initiated by atmospheric radicals at the M06-2X/D3/aug-cc-pVTZ level of theory (kcal/mol). (a) Cl_2HC– group, IM1. (b) –OCH_3 group, IM2.

320

In turn, as expected for this kind of reaction, the addition of O_2 to **IM2** to form the peroxy radical **IM2O$_2$** is barrierless (*-30.3[-32.8]* kcal/mol). Once the alkoxy radical **IM2O** is formed, it has three possible reaction routes:

(1) decomposition to **P3** and the $Cl_2CHC(O)O^{\bullet}$ intermediate radical (**IM5**), which is endothermic by *24.7[22.4]* kcal/mol relative to **IM2O**. The subsequent decomposition of **IM5** to form **P2** and $Cl_2{}^{\bullet}CH$ radical (**IM6**) is barrierless (*-42.4 [-43.6]* kcal/mol), the latter will produce **P1** and $HO_2^{\bullet}$ radical through O_2 addition, RO_2 recombination and H-abstraction by O_2.

(2) α-ester rearrangement, internal H-migration from C3 to carbonyl oxygen at C2 by a five membered transition state (**TS2-1**, *-21.2[-22.4]* kcal/mol) forming **IM7**. The latter decomposes through an O–C bond cleavage (**TS2-2**, *-38.4[-42.0]* kcal/mol) to dichloroacetic acid ($Cl_2CHC(O)OH$, **P4**) and $^{\bullet}C(O)H$ radical (**IM8**) which reacts with O_2 to give carbon monoxide (CO, **P5**) and $HO_2^{\bullet}$ radical. The transition state **TS2-1** for hydrogen shifting is about *16* kcal/mol above **IM2O,** while **TS2-2** is below **IM2O** and has a barrier of *10.8[9.1]* kcal/mol from **IM8**. Both **P4** and **P5** are formed merely by the channel of hydrogen abstraction in $–OCH_3$, both were identified experimentally with yields of *44* and *41*% respectively. (3) Reaction with O_2, producing dichloroacetic formate ($Cl_2CHC(O)OCHO$, **P6**) and $HO_2^{\bullet}$ radical. **P6** can also decompose through a transition state for H-shifting with simultaneous CO loss (**TS2-3**, *-41.7[-46.2]* kcal/mol) to identified products **P4** and **P5**.

In the experimental conditions, both dichloroacetic acid (**P4**) and carbon monoxide (**P5**) were positively identified and quantified experimentally as reaction products with similar yields, in agreement with the postulated degradation pathway as well as for P1 in the reaction with chlorine atoms the yield of **P4** and **P5** drops to *24* and *16*% respectively, a fact that can be explained because of the relative importance of the α-ester rearrangement pathway in the presence of NO_x over the molecular channel of the reaction with

343 O_2.[30] Although the proposed mechanism (**Figure 7**) for the intermediates formed once hydrogen
344 abstraction takes place is based solely on energy profiles and without kinetic analysis is purely speculative,
345 it is in good agreement with the experimentally identified products, which is the objective of this section.
346 A more detailed kinetic analysis is beyond the scope of this work.

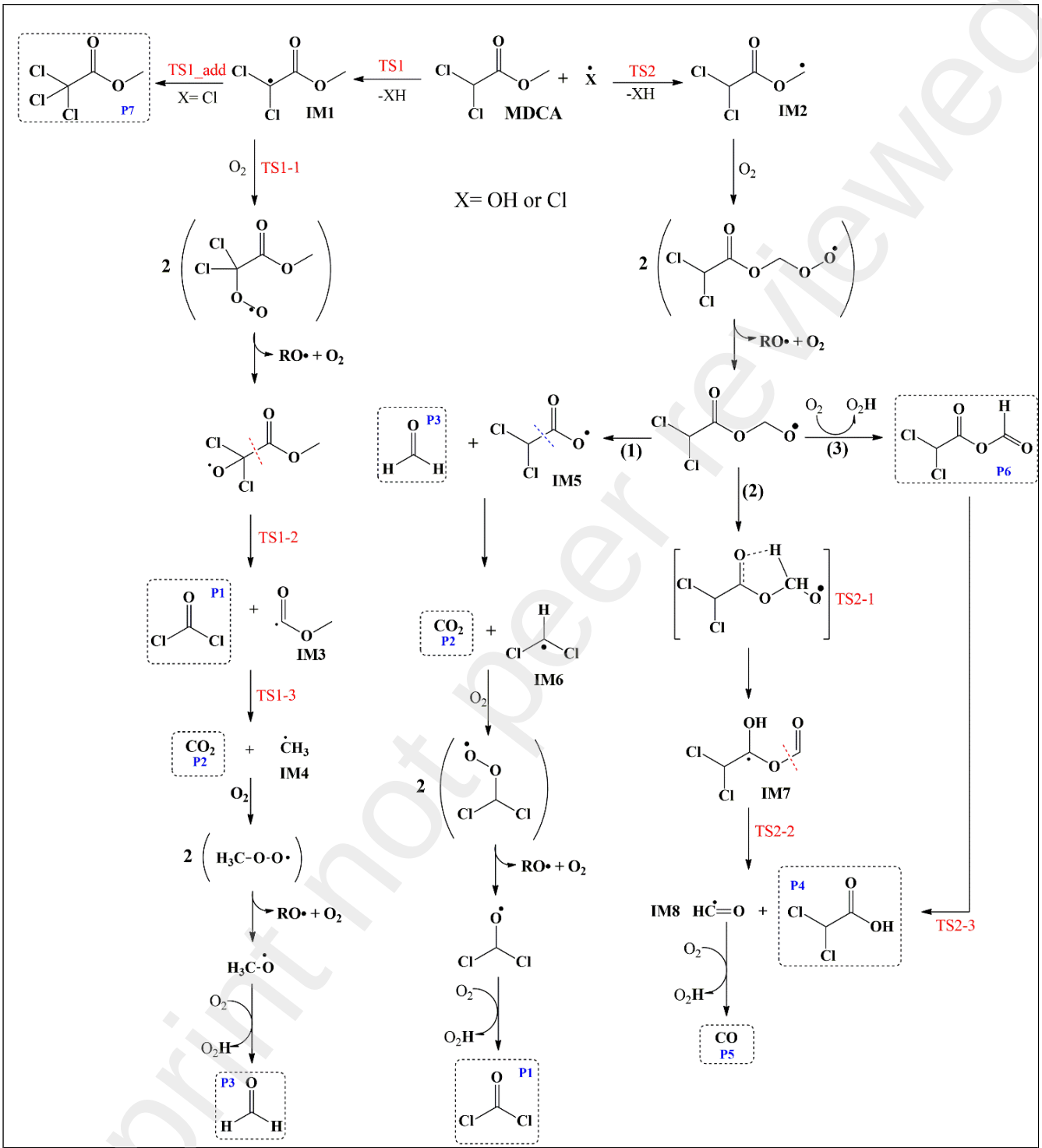

Figure 7 General proposed mechanism for gas phase oxidation MDCA initiated by atmospheric radicals (X=OH, Cl).

4. Atmospheric implications

The oxidation reactions involving tropospheric oxidants such as •OH radicals, •Cl atoms, O_3 molecules, or •NO_3 radicals can be used to calculate the residence time. Using the estimated rate coefficients and average tropospheric oxidant concentrations, the tropospheric lifetime (τ) is calculated with the expression; $\tau = 1/k_{MDCA} \times$[Oxidants]. where the concentrations of OH radicals and Cl atoms are reported as follows, [OH] = 2.0×10^6 radicals/cm^3 for about *12* hours(Hein et al., 1997) and [Cl] = 3.3 ± 1.1×10^4 atoms/cm^3 for *24* hours.(Wingenter et al., 1996) The atmospheric lifetimes obtained were then $\tau_{OH=}$ *4.76* and τ_{Cl}= *14.43* days respectively (see the SI). These values were calculated using the corresponding rate coefficients estimated in this work.

Since MDCA contains chlorine atoms itself, it could contribute to the increase of halogens in the stratosphere, thus promoting the destruction of the ozone layer. Therefore, the Ozone Depletion Potential (ODP) was calculated, resulting in a value of *0.0002*, significantly smaller than the reference trichlorofluoromethane, due to a shorter residence time. This fact reflects that the relative influence of this chlorinated organic compound on the destruction of the ozone layer is less than that of $CFCl_3$.

Other parameters to evaluate the possible impact of the emission of MDCA are the Photochemical Ozone Creation Potential (POCP) and the Acidification Potential (AP), see **Table S8**. The POCP value determined for MDCA, on the basis of a value of *100* for the POCP of ethene(Jenkin, 1998) was *14.62*. This low value confirms that the contribution of MDCA to tropospheric ozone formation will be negligible due to its relatively low reactivity.[29]

The resulting products of the oxidation of MDCA, phosgene and dichloroacetic acid, may have harmful impacts on the ozone layer or in the atmosphere. Phosgene is a highly toxic gas that has significant atmospheric implications. Exposure to phosgene can have serious health effects, including respiratory irritation, pulmonary edema, delayed symptoms, and long-term effects.(Pauluhn, 2021) This gas is a

potent air pollutant and contributes to poor air quality. Phosgene can react with atmospheric water vapour to form HCl and CO_2, which can contribute to acid rain and air pollution in the area of therelease.(Hantson et al., 1996) Its release into the atmosphere can lead to the formation of photochemical smog, and it has been identified as a potent ozone-depleting substance.(Harrison et al., 2019)

On the other hand, dichloroacetic acid is an acidic compound, and if it reacts with atmospheric water vapor or clouds, it can contribute to the formation of acid rain. Acid rain, as is well-known, can have detrimental effects on vegetation, ecosystems, and water bodies. MDCA is therefore an example of a species in which oxidation products are more detrimental to the troposphere health than the chemical itself. In order to verify the atmospheric implications of the identified products, it is possible to calculate the parameters AP, ODP, POCP and τ_{OH}. To do this, we use the value of the rate coefficient reported by Atkinson et al. 2001, for the reaction of phosgene with OH radicals= (5.00×10^{-15} cm^3/molecule·s). The values obtained were: ODP=0.048, AP=0.647, τ_{OH} =3.17 years, and POCP = 0 All calculated values are greater than the values determined for MDCA. Less POCP since phosgene does not have C-C and C-H bonds. Regarding dichloroacetic acid, no available data were found for the rate coefficient, thus hindering the calculation of its values.

5. Conclusions

The primary products of the reaction of MDCA with •OH radicals in simulated atmospheric conditions have been identified for the first time and the yields determined using *in-situ* FTIR techniques, adding to our previous experimental study of the reaction of MDCA with •Cl radicals. Moreover, a theoretical study of both reactions led to a proposed mechanism of the gas-phase degradation of this species.

Based on the results found, we can state that if H-abstraction occurs mainly on the Cl_2HC– group, reaction path (1), then **IM1** intermediate is generated that further reaction with O_2 will produce Cl_2CO **(P1**), CO_2

(**P2**) and H_2CO (**P3**). On the other side, if the H-abstraction occurs on the $–OCH_3$ group, path (2), then the oxidation of the intermediate **IM2** will produce $Cl_2CHC(O)OH$ (**P4**) and CO (**P5**).

The global rate coefficient calculated for the reaction with chlorine atoms overestimates the experimental value by about 20 times, despite energy corrections with the SVECV-f12 composite method on the M06 geometries reducing the rate constant value by about 25%. The rate coefficients obtained for the reaction with OH agree with those calculated previously. We found that including anharmonicity does not improve the value of the rate constant. Moreover, it greatly increases the time required for the calculation, making it impractical to use for systems with a greater number of atoms. The calculated branching ratio for the reaction with OH radicals were 88% and 12% for $Cl_2HC–$ and $–OCH_3$, respectively, while in the reaction with chlorine atoms, the branching ratio is 10% and 90%. This suggests that while in the reactions with OH radicals the reaction occurs mainly by the $Cl_2HC–$ group, on the reaction with Cl atoms most of the reaction would go through the abstraction from the $–OCH_3$ group.

The proposed mechanism based on energy profiles, agrees with the the product yields for the reaction with OH radical determined in this work for $Cl_2CHCOOH$ (*44* ± *3*%), $COCl_2$ (*43* ± *3*%), and CO (*41* ± *6*%) the energetics suggest that possibly the formation **P1** occurs mainly by path (1) since in path (2) the formation of **P4** and **P5** are more favorable. The thermodynamic and kinetics suggest that in reaction with •OH radicals the H-atom abstraction occurs preferably by $Cl_2HC–$ group.

In the Cl-initiated oxidation of MDCA, Straccia et al.(Straccia C et al., 2023) reported yields of (*24* ± *2*)% for $Cl_2CHCOOH$, (*19* ± *3*)% for CCl_2O, (*44* ± *2*)% for $Cl_3CCOOCH_3$, and (*16* ± *1*)% for CO, in good agreement with the proposed mechanism and thermodynamic values. Although, according to the kinetics, this reaction suggest that path (2) is favored over path (1). It is possible that the high yield for $Cl_3CCOOCH$ formation is related to thermodynamically favored **IM1** intermediary. The yields for the dichloroacetic

acid and phosgene determined in this work for the reaction with OH radicals are proximally half of the values found in the reaction with Cl atoms. These occur due to the formation of an intramolecular hydrogen transfer complex in the reactions of OH radicals with compounds containing carbonyl groups. A hydrogen bond is formed in the pre-reactive complex between the hydrogen atom of the •OH radical and the O atom of the C=O group. In the evolution on the reaction path, a second hydrogen bond is formed between the O atom of the •OH radical and an H atom on one of the terminal groups, resulting in a cyclic transition state. On the contrary, this stabilization is not present in the reaction initiated by •Cl atoms. The five-membered transition state reduces the activation barrier for the H-atom rearrangement to produce the carboxylic acid, resulting in a faster reaction.

The previous information was used to examine the atmospheric impact of MDCA. The calculated ODP value shows that the relative impact of MDCA on ozone depletion is lower than the reference compound $CFCl_3$. Also, the POCP was evaluated and a value of *14.62* was found. This low value confirms that the contribution of MDCA to tropospheric ozone formation will be negligible. The residence time estimated for MDCA is around days it would have a local impact.

Acknowledgments

V.G.S.C wishes to acknowledge CONICET for a doctoral fellowship and support. A.L.C. acknowledges CSIC (Uruguay) and ANII (Uruguay) for a postdoctoral fellowship and support. M. B. B. wishes to acknowledge the Alexander von Humboldt Foundation for financial support. M. A. T. wish to acknowledge to EUROCHAMP 2020, FONCyT, CONICET and SECyT UNC, Argentina. O.N.V. thank Pedeciba (Uruguay), CSIC (Uruguay) and ANII (Uruguay) for continuing support to the research in their group. molculations reported in this paper were carried out using the ClusterUY (site: https://cluster.uy), the cluster at the CCBG (Uruguay), and at the CCAD-UNC, which is part of SNCAD-MinCyT, Argentina.

437 **Supplementary information**

438 Supplementary information related to this article can be found at

439

440

References

Adler, T.B., Knizia, G., Werner, H.-J., 2007. A simple and efficient CCSD(T)-F12 approximation. J. Chem. Phys. 127, 221106. https://doi.org/10.1063/1.2817618

Atkinson, R., 2007. Rate constants for the atmospheric reactions of alkoxy radicals: An updated estimation method. Atmos. Environ. 41, 8468–8485. https://doi.org/10.1016/j.atmosenv.2007.07.002

Barnes, I., Becker, K.H., Mihalopoulos, N., 1994. An FTIR product study of the photooxidation of dimethyl disulfide. J. Atmospheric Chem. 18, 267–289. https://doi.org/10.1007/BF00696783

Bossolasco, A., Faragó, E.P., Schoemaecker, C., Fittschen, C., 2014. Rate constant of the reaction between CH3O2 and OH radicals. Chem. Phys. Lett. 593, 7–13. https://doi.org/10.1016/j.cplett.2013.12.052

Canneaux, S., Bohr, F., Henon, E., 2014. KiSThelP: A program to predict thermodynamic properties and rate constants from quantum chemistry results †. J. Comput. Chem. 35, 82–93. https://doi.org/10.1002/jcc.23470

Eckart, C., 1930. The Penetration of a Potential Barrier by Electrons. Phys. Rev. 35, 1303–1309. https://doi.org/10.1103/PhysRev.35.1303

Faragó, E.P., Schoemaecker, C., Viskolcz, B., Fittschen, C., 2015. Experimental determination of the rate constant of the reaction between C 2 H 5 O 2 and OH radicals. Chem. Phys. Lett. 619, 196–200. https://doi.org/10.1016/j.cplett.2014.11.069

Finlayson-Pitts, B.J., Pitts Jr, J.N., 1999. Chemistry of the upper and lower atmosphere: theory, experiments, and applications. Elsevier.

Fittschen, C., Whalley, L.K., Heard, D.E., 2014. The Reaction of CH3O2 Radicals with OH Radicals: A Neglected Sink for CH3O2 in the Remote Atmosphere. Environ. Sci. Technol. 48, 7700–7701. https://doi.org/10.1021/es502481q

Frisch, M. ea, Trucks, G.W., Schlegel, H.B., Scuseria, G.E., Robb, M.A., Cheeseman, J.R., Scalmani, G., Barone, V., Petersson, G.A., Nakatsuji, H., 2016. Gaussian 16, revision C. 01.

Gnanaprakasam, M., Sandhiya, L., Senthilkumar, K., 2018. Theoretical Investigation on the Mechanism and Kinetics of Atmospheric Reaction of Methyldichloroacetate with Hydroxyl Radical. J. Phys. Chem. A 122, 9316–9325. https://doi.org/10.1021/acs.jpca.8b05223

Goerigk, L., Hansen, A., Bauer, C., Ehrlich, S., Najibi, A., Grimme, S., 2017. A look at the density functional theory zoo with the advanced GMTKN55 database for general main group thermochemistry, kinetics and noncovalent interactions. Phys. Chem. Chem. Phys. 19, 32184–32215. https://doi.org/10.1039/C7CP04913G

Grimme, S., 2019. Exploration of Chemical Compound, Conformer, and Reaction Space with Meta-Dynamics Simulations Based on Tight-Binding Quantum Chemical Calculations. J. Chem. Theory Comput. 15, 2847–2862. https://doi.org/10.1021/acs.jctc.9b00143

Grimme, S., Antony, J., Ehrlich, S., Krieg, H., 2010. A consistent and accurate *ab initio* parametrization of density functional dispersion correction (DFT-D) for the 94 elements H-Pu. J. Chem. Phys. 132, 154104. https://doi.org/10.1063/1.3382344

Hantson, P., Baud, F.J., Garnier, R., 1996. Toxic gases. Hum. Toxicol. 661–669.

Harrison, J.J., Chipperfield, M.P., Hossaini, R., Boone, C.D., Dhomse, S., Feng, W., Bernath, P.F., 2019. Phosgene in the Upper Troposphere and Lower Stratosphere: A Marker for Product Gas Injection Due to Chlorine-Containing Very Short Lived Substances. Geophys. Res. Lett. 46, 1032–1039. https://doi.org/10.1029/2018GL079784

Hein, R., Crutzen, P.J., Heimann, M., 1997. An inverse modeling approach to investigate the global atmospheric methane cycle. Glob. Biogeochem. Cycles 11, 43–76. https://doi.org/10.1029/96GB03043

Jenkin, M.E., 1998. Photochemical ozone and PAN creation potentials: Rationalisation and methods of estimation. AEA Technol. Plc AEAT Rep. 4182, 003.

Kieninger, M., Ventura, O.N., 2022. SVECV-f12: A composite scheme for accurate and cost-effective evaluation of reaction barriers II. Benchmarking using Karton's BH28 barrier heights database. Int. J. Quantum Chem. e27069. https://doi.org/10.1002/qua.27069

Knizia, G., Adler, T.B., Werner, H.-J., 2009. Simplified CCSD(T)-F12 methods: Theory and benchmarks. J. Chem. Phys. 130, 054104. https://doi.org/10.1063/1.3054300

Kohn, W., Sham, L., 1965. Self-Consistent Equations Including Exchange and Correlation Effects. J Phys Rev 140, 1133–1138. https://doi.org/10.1103/PhysRev.140.A1133

Litvinov, O.A., Zuev, M.B., Naumov, V.A., Volden, H.V., Hagen, K., 1993. Molecular structure and conformation of gas-phase methyl dichloroacetate. J. Phys. Chem. 97, 10674–10677. https://doi.org/10.1021/j100143a024

McClay, K., Schaefer, C.E., Vainberg, S., Steffan, R.J., 2007. Biodegradation of Bis(2-Chloroethyl) Ether by Xanthobacter sp. Strain ENV481. Appl. Environ. Microbiol. 73, 6870–6875. https://doi.org/10.1128/AEM.01379-07

Pauluhn, J., 2021. Phosgene inhalation toxicity: Update on mechanisms and mechanism-based treatment strategies. Toxicology 450, 152682. https://doi.org/10.1016/j.tox.2021.152682

Peterson, K.A., Adler, T.B., Werner, H.-J., 2008. Systematically convergent basis sets for explicitly correlated wavefunctions: The atoms H, He, B–Ne, and Al–Ar. J. Chem. Phys. 128, 084102. https://doi.org/10.1063/1.2831537

Pracht, P., Bohle, F., Grimme, S., 2020. Automated exploration of the low-energy chemical space with fast quantum chemical methods. Phys. Chem. Chem. Phys. 22, 7169–7192. https://doi.org/10.1039/C9CP06869D

Straccia C, V.G., Rivela, C.B., Blanco, M.B., Teruel, M.A., 2023. Kinetics and products study of the reaction of Cl atoms with methyl dichloroacetate: reactivity, mechanism, and environmental implications. Environ. Sci. Atmospheres 3, 872–881. https://doi.org/10.1039/D3EA00004D

Terao, K., 1992. α-Chlorocarbonyl Compounds: Their Synthesis and Applications (Commemoration Issue Dedicated to Professor Shigeo Tanimoto on the Occasion of His Retirement). Bull. Inst. Chem. Res. Kyoto Univ. 70, 338–377.

Ventura, O.N., Kieninger, M., Katz, A., Vega-Teijido, M., Segovia, M., Irving, K., 2021. SVECV-f12: Benchmark of a composite scheme for accurate and cost effective evaluation of reaction barriers. Int. J. Quantum Chem. 121. https://doi.org/10.1002/qua.26745

Viegas, L.P., 2021. Simplified Protocol for the Calculation of Multiconformer Transition State Theory Rate Constants Applied to Tropospheric OH-Initiated Oxidation Reactions. J. Phys. Chem. A 125, 4499–4512. https://doi.org/10.1021/acs.jpca.1c00683

Werner, H.-J., Knowles, P.J., Manby, F.R., Black, J.A., Doll, K., Heßelmann, A., Kats, D., Köhn, A., Korona, T., Kreplin, D.A., Ma, Q., Miller, T.F., Mitrushchenkov, A., Peterson, K.A., Polyak, I., Rauhut, G., Sibaev, M., 2020. The Molpro quantum chemistry package. J. Chem. Phys. 152, 144107. https://doi.org/10.1063/5.0005081

Wingenter, O.W., Kubo, M.K., Blake, N.J., Smith, T.W., Blake, D.R., Rowland, F.S., 1996. Hydrocarbon and halocarbon measurements as photochemical and dynamical indicators of atmospheric hydroxyl, atomic chlorine, and vertical mixing obtained during Lagrangian flights. J. Geophys. Res. Atmospheres 101, 4331–4340. https://doi.org/10.1029/95JD02457

Woon, D.E., Dunning, T.H., 1995. Gaussian basis sets for use in correlated molecular calculations. V. Core-valence basis sets for boron through neon. J. Chem. Phys. 103, 4572–4585. https://doi.org/10.1063/1.470645

Woon, D.E., Dunning, T.H., 1993. Gaussian basis sets for use in correlated molecular calculations. III. The atoms aluminum through argon. J. Chem. Phys. 98, 1358–1371. https://doi.org/10.1063/1.464303

Yu, H.S., He, X., Li, S.L., Truhlar, D.G., 2016. MN15: A Kohn–Sham global-hybrid exchange–correlation density functional with broad accuracy for multi-reference and single-reference systems and noncovalent interactions. Chem. Sci. 7, 5032–5051. https://doi.org/10.1039/C6SC00705H

Zhao, Y., Truhlar, D.G., 2008. The M06 suite of density functionals for main group thermochemistry, thermochemical kinetics, noncovalent interactions, excited states, and transition elements: two new functionals and systematic testing of four M06-class functionals and 12 other functionals. Theor. Chem. Acc. 120, 215–241. https://doi.org/10.1007/s00214-007-0310-x

Theoretical and FTIR study of the atmospheric reaction of methyl dichloroacetate with •OH and Cl• radicals: kinetics, products, and mechanism.

Vianni G. Straccia C.[1], Alejandro L. Cardona[2], María B. Blanco[1,3], Cynthia B. Rivela[1], Mariano A. Teruel[1]*, and Oscar N. Ventura[2]*

1 Laboratorio Universitario de Química y Contaminación del Aire (L.U.Q.C.A.). Instituto de Investigaciones en Fisicoquímica de Córdoba (I.N.F.I.Q.C.), CONICET, Dpto. de Fisicoquímica, Facultad de Ciencias Químicas, Universidad Nacional de Córdoba. Ciudad Universitaria, 5000 Córdoba, Argentina.

2 Computational Chemistry and Biology Group (CCBG), DETEMA, Facultad de Química, UdelaR, Montevideo, Uruguay.

3 Institute for Atmospheric and Environmental Research, University of Wuppertal, DE-42097 Wuppertal, Germany.

Corresponding authors:

Prof. Dr. Mariano A. Teruel
Laboratorio Universitario de Química y Contaminación del Aire (L.U.Q.C.A.).
Instituto de Investigaciones en Fisicoquímica de Córdoba (I.N.F.I.Q.C.), CONICET,
Dpto. de Fisicoquímica, Facultad de Ciencias Químicas,
Universidad Nacional de Córdoba. Ciudad Universitaria,
5000 Córdoba, Argentina.
e-mail: mariano.teruel@unc.edu.ar

Prof. Dr. Oscar N. Ventura
Computational Chemistry and Biology Group (CCBG),
DETEMA, Facultad de Química, UdelaR,
Isidoro de María 1610, Piso 4º
11800 Montevideo, Uruguay.
e-mail: oscar.n.ventura@gmail.com

Both authors Vianni G. Straccia C. and Alejandro L. Cardona have contributed equally to this work and must be regarded as first authors.